RSC Advances

PAPER

View Article Online
View Journal | View Issue

Cite this: *RSC Adv.*, 2023, **13**, 20040

Aptamer-based colorimetric and lateral flow assay approaches for the detection of toxic metal ions, thallium(I) and lead(II)†

Sathya Srinivasan,[ab] Velu Ranganathan,[a] Erin M. McConnell,[a] Bhaskar Mohan Murari*[c] and Maria C. DeRosa*[a]

Received 13th March 2023
Accepted 14th June 2023

DOI: 10.1039/d3ra01658g

rsc.li/rsc-advances

Thallium(I) and lead(II) ions are heavy metals and extremely toxic. These metals are environmental pollutants, posing a severe risk to the environment and human health. In this study, two approaches were examined using aptamer and nanomaterial-based conjugates for thallium and lead detection. The first approach utilized an in-solution adsorption–desorption approach to develop colorimetric aptasensors for the detection of thallium(I) and lead(II) using gold or silver nanoparticles. The second approach was the development of lateral flow assays, and their performance was tested with thallium (limit of detection is 7.4 μM) and lead ion (limit of detection is 6.6 nM) spiked into real samples. The approaches assessed are rapid, inexpensive, and time efficient with the potential to become the basis for future biosensor devices.

1. Introduction

The monitoring of toxic metal ions is required in marine ecosystems, as these pollutants jeopardize both human health and the environment.[1–3] Indeed, the Environmental Protection Agency (EPA) and the international World Health Organization regulations delimit acceptable Pb levels in drinking water as 10 ppb and 50 ppb, respectively.[4,5] The Centers for Disease Control and Prevention define the acceptable level of Pb in blood as 10 μg dL^{-1} (301.9 nM).[6] The EPA delineates a maximum acceptable level of <2.5 to 10 nM Tl ions for drinking water, while surface-water can reach ~100 nM.[7] Concentrations of 1–88 ppm (5–440 μM) of thallium have been noted in metal mining drainage river zones.[3] Unfortunately, even small amounts of Tl and Pb could cause serious health concerns.[3] Hence, metal detection is significant for environmental and biological applications. Current detection methods like emission spectrometry, atomic absorption, and ICP-MS, have been extensively used for detection of metal ions.[8] These approaches rely on expensive instruments, and time-consuming and complicated pretreatment processes.[9] Thus, rapid, sensitive, low-cost and simple techniques for detecting toxic metal ions are in great demand.[10]

Silver nanoparticles (AgNPs) and gold nanoparticles (AuNPs) have been used in several biosensors as tags to replace modification with chromophores or enzymes. Specifically, AuNPs are used in almost every biological application of metallic nanoparticles because of their chemical and physical properties such as resistance to oxidation, ease of synthesis, distance, shape and size – dependent optical properties. The most familiar of these interesting optical features is the red to blue color change upon aggregation.[11,12] AgNP and AuNP solutions appear yellow and red in color, respectively, due to the Localized Surface Plasmon Resonance (LSPR) phenomenon. Those colors change from red to blue for AuNPs and yellow to orange for AgNPs in response to aggregation state and refractive index changes on the metal nanoparticle surface. This can be exploited to develop naked-eye detectable colorimetric methods that have been broadly recognized for their practicality and simplicity.[13,14]

Aptamers are synthetic single-stranded RNA or DNA oligonucleotides able to bind to target molecules with high affinity and selectivity showing many advantages over antibodies and offering a broad range of benefits of development, production, and commercial application.[15,16] The process for finding aptamers, SELEX, can be adapted for the selection of aptamers that bind to a variety of target molecules[17] including cells,[18] viruses,[19] proteins,[20] as well as small molecules such as vitamins,[21] toxins[15] and antibiotics.[22] Aptamers have exhibited great flexibility in the design of various biosensors like colorimetric, fluorescence and electrochemical, sensing methods[23–28] that undergo different conformational changes upon binding their target.

Lateral flow assays (LFAs) are widely applicable technology, which can be altered for the detection of different targets without instrumentation. Their user-friendly design, low cost,

[a]*Department of Chemistry, Carleton University, 1125 Colonel By Drive, Ottawa, ON K1S 5B6, Canada. E-mail: maria.derosa@carleton.ca; Tel: +1-613-520-2600 ext. 4388*
[b]*Department of Biotechnology, School of Bioscience and Technology, VIT, Vellore, 632 104, TN, India*
[c]*Department of Sensor and Biomedical Technology, School of Electronics Engineering, VIT, Vellore, 632 104, TN, India*

† Electronic supplementary information (ESI) available. See DOI: https://doi.org/10.1039/d3ra01658g

easy storage and compactness make them ideal for on-site sample analysis. Results are quick and easily interpretable by both non-specialists and specialists.[29,30] The potential of LFAs as a widely available tool has been recently demonstrated by the rapid antigen tests used to mitigate the COVID-19 pandemic. Of particular relevance, LFAs have been developed for mycotoxins,[31–33] small molecules such as kanamycin,[34] ATP and cocaine[35] and heavy metal like Hg(II).[36]

In this article, two methodologies were investigated for toxic metal ions, both in lateral flow and solution assays. The first approach was a solution-based adsorption–desorption colorimetric approach wherein the aptamer–AuNP complex was prepared by electrostatic interaction in-between the aptamer and AuNPs in the absence of target. Desorption of aptamer from the AuNP surface occurred in the addition of metal ions as they preferentially interact with the aptamer, displacing the AuNPs. The presence of NaCl then persuaded the AuNP to aggregate, leading to the solution color changing from red to blue (Fig. 1A). A similar mechanism was explored involving the AgNP colorimetric detection of metal ion and the solution color changing from yellow to orange. The last approach was an adsorption–desorption colorimetric LFA. Without target available, biotin-functionalized-aptamer coated the AuNPs surface and the aptamer coated AuNPs were captured by streptavidin at test zone. Accumulation of aptamer–AuNP complex on the test line resulted in red coloured dot formation. Red color was also expected at the control line due to non-specific interaction between poly diallyl dimethyl ammonium chloride (PDDA) and the AuNP complexes. Upon the addition of ion, the ion preferentially interacted with the biotin-modified aptamer and was captured (without the AuNPs) by streptavidin. In this case, no red colored dot appeared at the test zone due to the lack of gold nanoparticles. However, red color remained at the PDDA control line through non-specifically bound AuNPs (Fig. 1B). These lateral flow and colorimetric assays are rapid, inexpensive, and simple to perform with the potential to become the basis for future biosensor.

2. Materials and methods

Gold(III) chloride hydrate, human serum type AB (male), silver nitrate, $NaBH_4$, thallium(I) chloride, cesium(I) chloride, rubidium(I) chloride, sodium chloride, magnesium(II) chloride, iron(III) nitrate, potassium(I) chloride, lead(II) nitrate, silver(I) nitrate, lithium(I) chloride, nickel(II) nitrate, streptavidin, PDDA (15%), zinc(II) nitrate and mercury(II) nitrate cadmium chloride(II) were purchased from Sigma-Aldrich, Canada. Phosphoramidites dmf-dG-CE, dT-CE, dA-CE, Ac-dC-CE and biotin modifier were purchased from Glen Research, USA. ACN, TEAA, and anhydrous acetonitrile were purchased from BDH, VWR, Canada. Sample and absorption pad (CFSP223000) obtained from Millipore Co, Bedford, MA. Pullulan bought from Polysciences, Warrington, PA. NC membrane was purchased from Sartorius Stedim Biotech, Germany and conjugate pad was purchased from Ahlstrom Munksjo, Finland. The aptamers used in this study were reported in the literature[7,37,38] and the aptamers were included in the ESI Table S1.†

2.1 Instruments

UV/vis spectra were recorded using a CARY 300 Bio spectrophotometer (Varian, USA), TEM images were obtained using a FEI Tecnai F20 FETEM. The dispensing platform of BIODOT: ZX 1000 was used for LFAs. Quantitative analysis was measured using the ImageJ software.[39]

2.2 High resolution TEM analysis

TEM images with and without Tl(I) and Pb(II) ions, were observed by drop-casting 10 μL of metal nanoparticles–aptamer complexes on a copper grid (carbon coated). More details included in the ESI.†

2.3 Colorimetric solution preparation

5′-Biotin-labelled aptamer (6 μL of 10 μM in water) and AuNPs solution (100 μL of 11.60 nM) were mixed and kept for 15 minutes.

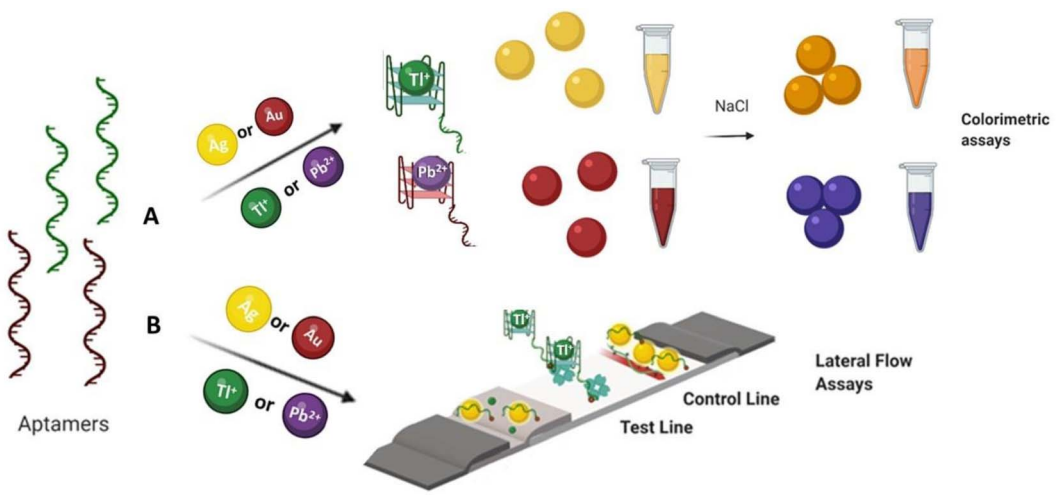

Fig. 1 Schematic illustration of (A) colorimetric and (B) lateral flow assay approaches for the detection of Tl(I) and Pb(II) ions.

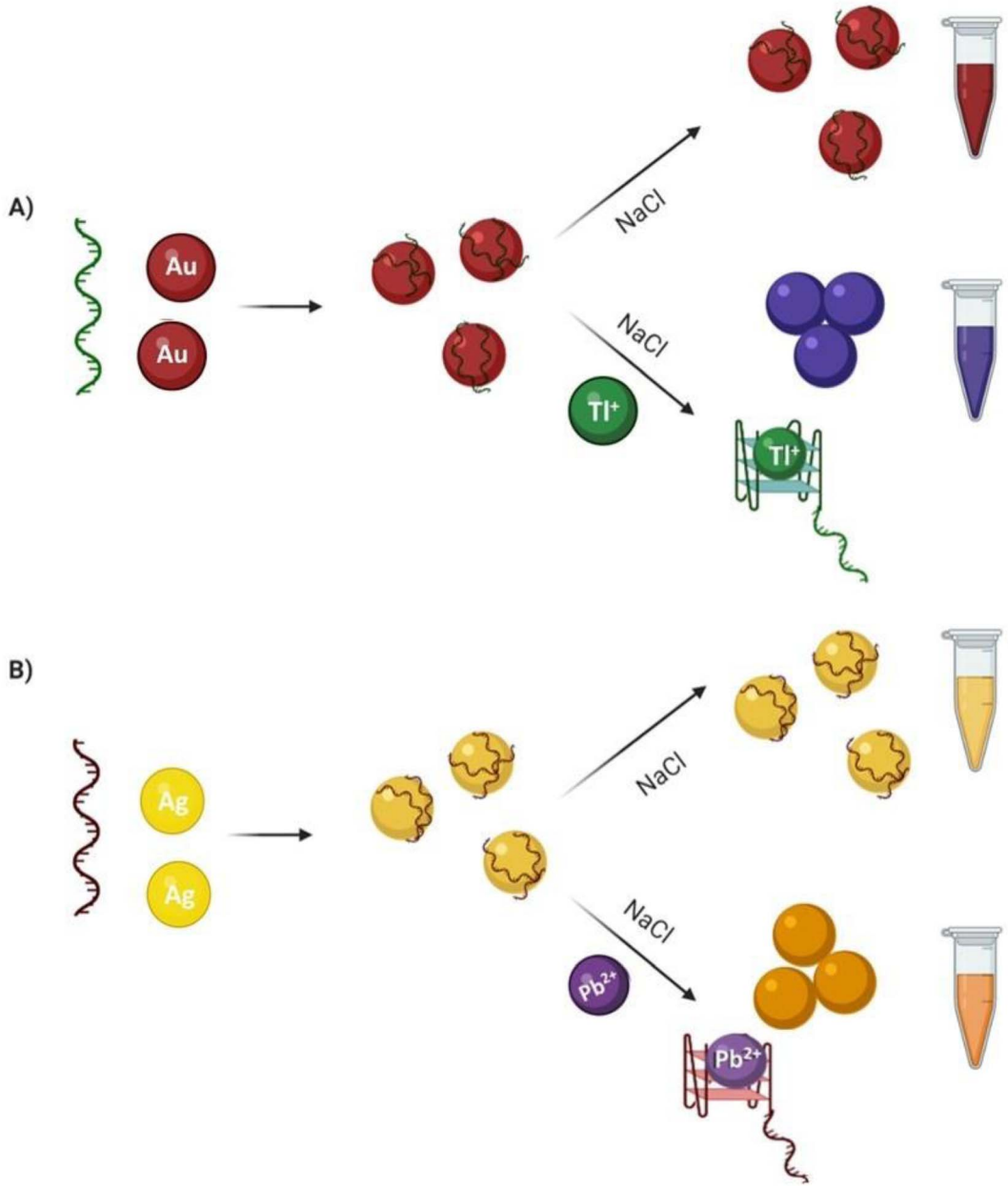

Fig. 2 Schematic illustration of colorimetric assays: (A). AuNPs based adsorption–desorption colorimetric detection mechanism, shown here for Tl(I) but the same mechanism applies to Pb(II). (B). AgNPs based adsorption–desorption colorimetric detection mechanism, shown here for Pb(II) but the same mechanism applies for Tl(I).

Then, different concentrations of target ranging from 3.3 μM to 120 μM for thallium and 6.6 nM to 150 nM for Lead were mixed in the solution, vortexed briefly, and kept for 15 minutes. NaCl (50 μL of 0.5 M) was slowly mixed into the above solution where the spectral and color changes were noted. The AgNP colorimetric solution assays were prepared using the similar conditions.

2.4 LFA preparation

LFA samples of toxic metal ions in distilled H_2O, river water and serum (human) were prepared at different concentrations ranging from 3.3 μM to 120 μM for Thallium and 6.6 nM to 150 nM for lead. 5′-Biotin-labelled aptamer (6 μL of 10 μM in water) and AuNPs solution (100 μL of 11.60 nM) were mixed and kept for 15 minutes. Then, the different concentration of target ranging from 3.3 μM to 120 μM for thallium and 6.6 nM to 150 nM for lead, was added into tubes and the mixture was vortexed for 15 minutes. These sample solutions were added in LFA strip. The peak areas were evaluated with the ImageJ software. The AgNP colorimetric LFAs were prepared using the same experimental conditions.

2.5 Construction of a lateral flow assay strip

LFAs constructed by overlapping four LFA pads namely the absorption pad, sample pad, conjugate pad and NC membrane.

A width of 5 mm LFA pads cut and pasted on an adhesive backing with a 2 mm overlap. The sample and conjugate pads were made from fiberglass. NC membrane was used to immobilize PDDA (15% PDDA polymer, 2 μL cm^{-1}), and Streptavidin as a capture reagent (2.5 mg mL^{-1}, 0.5 μL) at different locations to develop the control and test zones respectively. The distance between the zones is approximately 4 mm. The device was loaded with reagent and dried for 30 minutes at room temperature prior to use. The test samples consist of the aptamer and Au nanoparticles in the presence and absence of target. The samples were applied to the strip (approximately 50 μL) where the sample solution travelled through the membrane for <1 minute before the device was read. No red color at the test zone indicated the target presence while red color at the test spot indicated the absence of target. Color at the control zone verified that Au nanoparticles migrated effectively across the lateral flow strip.

3. Results and discussion

3.1 Adsorption and desorption colorimetric method for heavy metal ions (solution studies)

We investigated a simple colorimetric approach that used a basic mechanism. The mechanism for metal ion detection is depicted in Fig. 2. The aptamer–AuNP complex was prepared through electrostatic attraction between the AuNPs and the aptamer.[40,41] A red colour with a strong absorption at 520 nm was observed in the aptamer–AuNPs solution and was attributed to the localized surface plasmon resonance.[42,43] Conformational change and aptamer desorption from the AuNP surface occurred in the presence of metal ion target. In the presence of salt, the AuNPs aggregates lead to the corresponding color change from red to blue (Fig. 3a). The increase in concentration of Tl(I) ions led to a shift towards longer wavelength (Fig. 4a). The ratio of the absorbance (A_{700}/A_{520}) was plotted *versus* different Tl(I) ions concentrations in the above solution (Fig. 4b) and showed an LOD of 9.0 μM for the AuNP based system. The adsorption–desorption mechanism for the AuNP and AgNP–aptamer complex in absence and presence of Tl(I) was supported by TEM (Fig. S6 and S7†). The selectivity experiments were performed over other metal ions including Mg(II), Rb(I), Cs(I), Na(I), Ag(I), Cd(II), K(I) and Li(I) under similar experimental methods and showed no noticeable color and spectral changes. These results indicate that the aptamer–AuNPs complex is selective for Tl(I) (Fig. S1a†). All the metal ions concentrations were 120 μM.

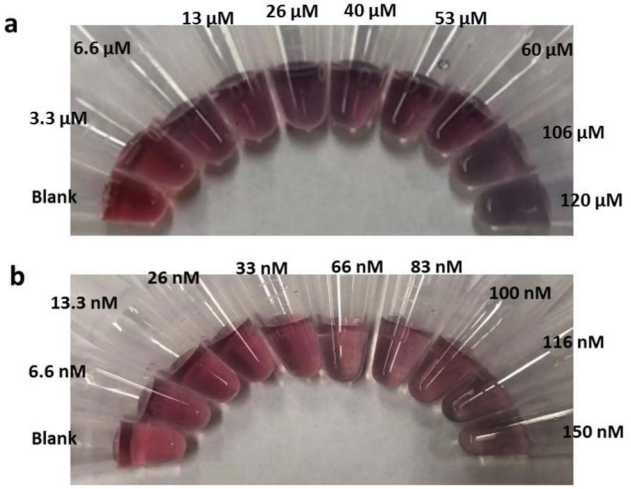

Fig. 3 (a). AuNP/Tl(I)–aptamer complex in the addition of increasing concentrations of Tl(I) ions (0–120 μM) and (b) Pb(II)–aptamer–AuNP complex with different concentrations of Pb(II) (0–150 nM). Visual colour changes occur from left to right.

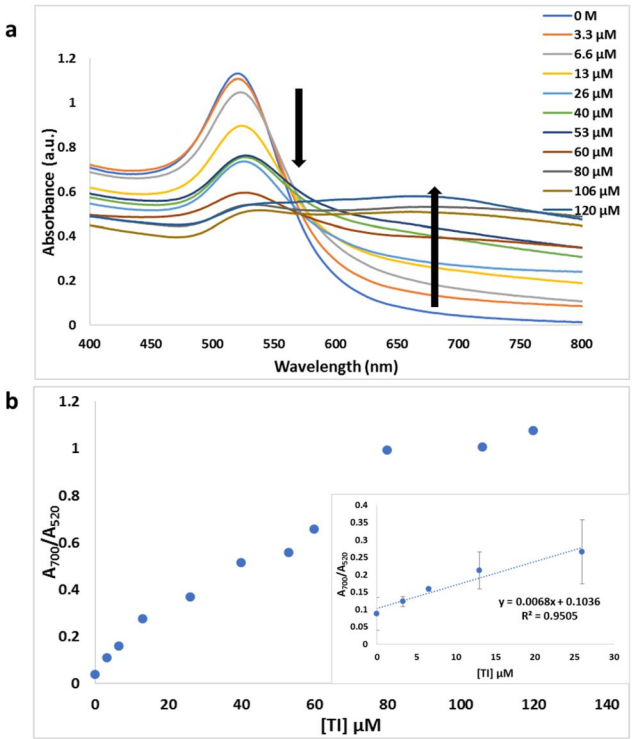

Fig. 4 (a) The UV-vis spectra of Tl–aptamer/AuNP complexes under varying concentrations of Tl(I) ions (0–120 μM). (b) The curve displays the ratio of optical density at 700 nm to 520 nm *versus* respective Tl(I) ion concentrations. The inset illustrates the linear dynamic range.

We performed the same experiments for the colorimetric aptasensor based detection of Pb. Results of the spectral and colour change studies were similar to experiments involving the AuNP colorimetric detection of Tl(I). In the presence of various concentrations of Pb(II) ions from 0 to 150 nM, the Pb(II)–aptamer preferentially bound to the Pb (aptamer–Pb complex) and resulted in visual and spectral changes as demonstrated in Fig. 3b and S2a.† This assay indicated a good linear range from 0 M to 33 nM Pb(II) with an LOD of 9.5 nM (Fig. S2b†). The selectivity for Pb ions towards other metal ions like Hg(II), Zn(II), Ag(I), Ni(II), Cd(II) and Fe(II) (Fig. S1b†) was confirmed. All the ion concentrations were 150 nM. Liu *et al.*,[44] have reported that arsenic (As(III)) cannot bind with its specific aptamer in the colorimetric method when they used arsenic-binding aptamer and AuNPs. As(III) adsorption to the AuNP surface occurred as opposed to specific binding with its arsenic binding aptamer,

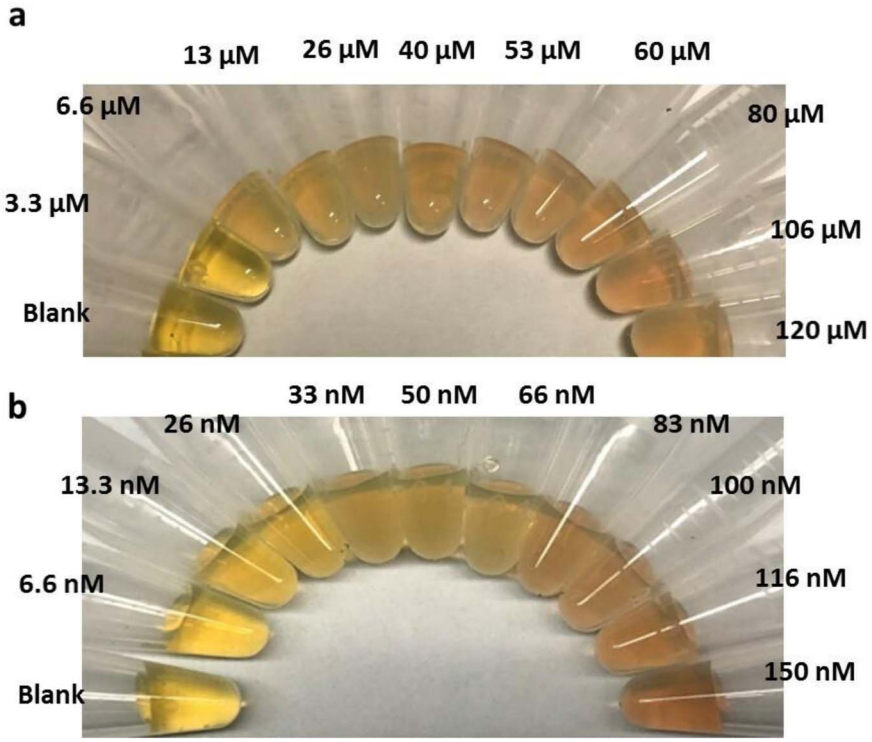

Fig. 5 (a) Tl(I)–aptamer/AgNP complex in the addition of varying concentrations of Tl(I) (0–120 μM) and (b) Pb(II)–aptamer–AgNP complex in the presence of increasing concentrations of Pb(II) ions (0–150 nM). Visual colour changes occur from left to right.

leading to AuNP aggregation. We performed colorimetric control experiments of Au and Ag nanoparticles without aptamer in the addition of the salt and metal ions, which can be found in Fig. S3.† The target-induced AuNP aggregation was tested by exposing the AuNPs to different concentrations of Tl(I). The results indicated that the color of the AuNPs solution was not affected which demonstrated that the Tl(I) did not induce the aggregation of AuNP on its own (Fig. S3a†). Upon the addition of NaCl, the AuNP visual color change from red to blue was due to the formation of nanoparticle aggregations (Fig. S3b†). Similar results are illustrated in Fig. S3c and S3d† for Pb(II) studies, while AgNP with different concentrations of Tl(I) or Pb(II) and salt yielded comparable results to the AuNP aggregation experiments; depicted in Fig. S3e–h.†

Concurrently, this colorimetric based Tl(I) and Pb(II) ion sensing method was adapted to use AgNPs, Tl(I)-binding aptamers, and Pb(II)-binding aptamer sequences as shown in Fig. 5. This approach yielded similar results to those discussed in the above paragraphs. In the presence of Tl(I) ions (concentrations 0–120 μM) there was specific binding of Tl(I) with its aptamer. The resulting AgNP surface plasmon absorption peak at 400 nm decreased with a gradual increase in a broad band at 480 nm (Fig. S4a†) and corresponding visual color change from yellow to brownish red is due to the formation of nanoparticle aggregates (Fig. 5a). The respective absorbances at 480 nm and 395 nm (A_{480}/A_{395}) provided good linearity and a calculated LOD of 3.17 μM when plotted as a function of various concentrations of Tl(I) ion. The inset shows the linear range from 0 M to 26 μM (Fig. S4b†). The selectivity experiments performed against various metal ions including Cs(I), Ag(I), Rb(I), Mg(II), Na(I), Li(I), Cd(II) and K(I) added to the solution containing aptamers–AgNPs complexes, were run under the same experimental conditions. No noticeable color or spectral changes were observed, indicating that the aptamer–AgNPs complex is selective for the Tl(I) (Fig. S5a†). A similar procedure was used for the colorimetric (aptamer–AgNPs) aptasensor for Pb providing comparable spectral and color change results to the AgNP colorimetric detection of Tl(I) experiments. Pb(II)–aptamer displayed preferential binding with Pb(II) ions (0–150 nM) and resulted in the spectral changes seen in Fig. 6a and 5b. This assay provided good linearity with a range of 0–33 nM Pb(II) and a calculated LOD of 5.6 nM (Fig. 6b). The selectivity for Pb(II) *versus* other metal ions like Hg(II), Zn(II), Ni(II), Ag(I), Cd(II) and Fe(II) (Fig. S5b†) were confirmed. The adsorption–desorption mechanism for the AuNP and AgNP–aptamer complex in absence and presence of their target metal ions was supported by TEM (Fig. S8 and S9†). In addition, the competitive titration experiments were done in the presence of 5-fold excess of other metal ions. In this case, there was a modest change in the color of the solutions with the other metals present, but the sensor was still responsive to Tl(I) concentrations. The figures have been included in the ESI in Fig. S17.†

3.2 Adsorption–desorption LFA

While the colorimetric method had the advantage of simplicity, sensitivity, and rapidity of results, which can be detected by naked eye, it had the disadvantage that a solution-based

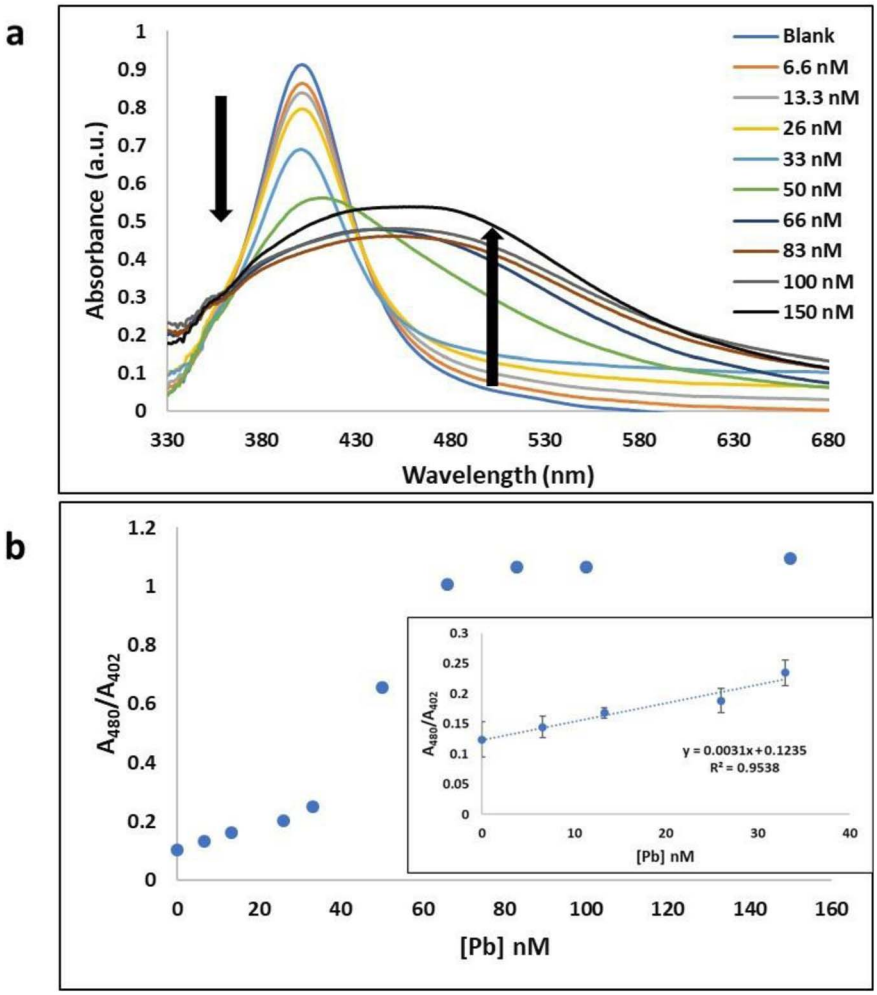

Fig. 6 (a) Pb–aptamer/AgNP complex absorption spectra under various concentrations of Pb(II) ions (0–150 nM). (b) The curve displays the absorbance ratio at 480 nm to 402 nm *versus* respective Pb(II) ion concentrations. The inset illustrates the linear dynamic range.

method is not always practical for field testing. This challenge was overcome by developing a lateral flow test. The principle of detection was based on LFA aptamer "adsorption–desorption" reaction (Fig. 7 a).[45,46] The test and control zones were immobilized streptavidin and a polycationic polymer (PDDA) respectively. When applied to the LFA without target, the biotin-functionalized-AuNP complex solution was captured by streptavidin. Accumulation of the AuNP–aptamer in the test spot results in the visualization of a red coloured dot. Red color is also expected within the PDDA control zone because of the electrostatic interaction of the AuNP–aptamer complexes with the polyelectrolyte. In the presence of various concentrations of Tl(I) ion (0–120 μM) the biotin-modified Tl(I) aptamer preferentially bound with Tl(I), preventing its immobilization on the surface of AuNP. The solution was applied to the LFA and the biotin-modified aptamer–Tl complex was stopped by streptavidin and the absence of red colored dot was noted on the test zone because of the lack of gold nanoparticles. A red color was still expected within the PDDA control zone through non-specifically bound AuNPs. We determined the sensitivity of adsorption–desorption LFA by measuring Tl at different concentrations. Test zone intensity progressively decreased with increasing Tl concentrations range from 0 M to 120 μM. A curve was plotted of the test zone (T) peak area (analyzed using ImageJ software) *versus* various TI concentrations. This showed linearity in the range from 0 M to 26 μM Tl with a calculated LOD of 7.4 μM (Fig. 7).

Similar experimental conditions were performed for the colorimetric LFA assays using AuNPs and Pb-binding aptamer for Pb(II) detection. LFA studies provided comparable results to previous AuNP based colorimetric LFA detection of Tl(I) experiments. The test zone (T) peak area was plotted against increasing Pb(II) concentrations in a calibration curve where it was determined to have good linearity (0–33 nM) with an LOD of 6.6 nM (Fig. S10†). The LFA selectivity experiments of Tl(I) were performed against different metal ions including Cs(I), Ag(I), K(I), Na(I), Li(I) and Rb(I) (Fig. 8a). The observations (reduced peak area for Tl(I)) indicated that the LFA is highly specific for Tl(I). Similarly, the LFA selectivity experiments for Pb(II) ions were performed with different metal ions Ni(II), Hg(II), Ag(I), Zn(II) and Fe(II) (Fig. 8b). The observations (reduced peak area for Pb(II)) indicated that the LFA is highly specific for Pb.

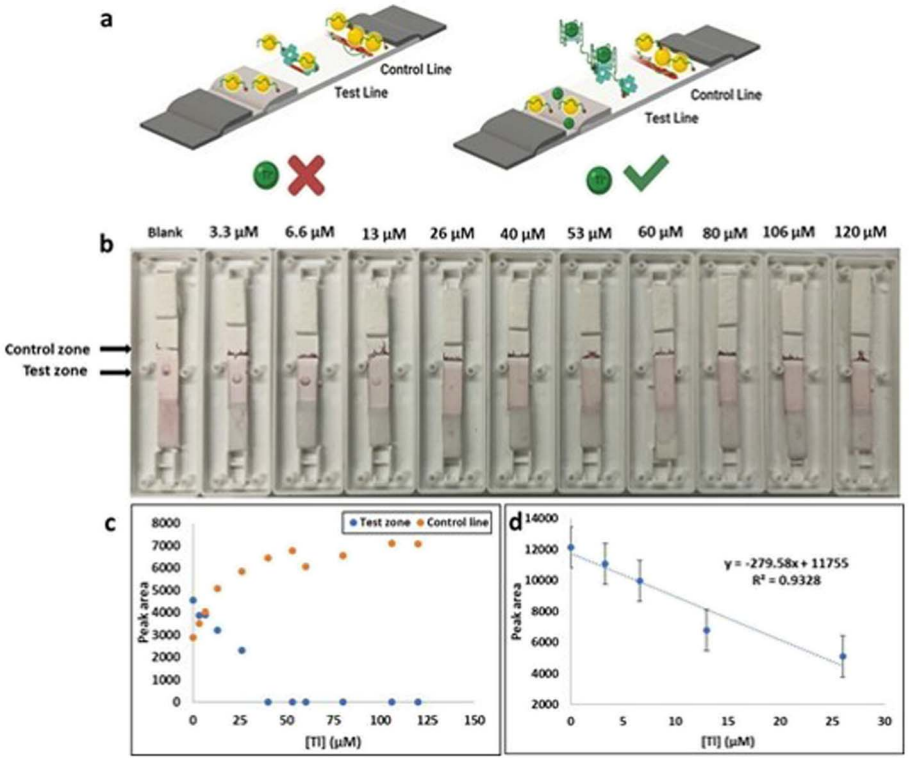

Fig. 7 (a) The adsorption and desorption method of colorimetric LFAs. (b) The LFA (AuNPs based) for Tl(I) detection with various concentrations of Tl(I) ions (ranges from 0–120 μM). (c) The curve was plotted against to the peak area control (c) and test (T) zones *vs.* various concentrations of Tl(I) were analyzed by ImageJ software. (d) Plot showing the linear dynamic range.

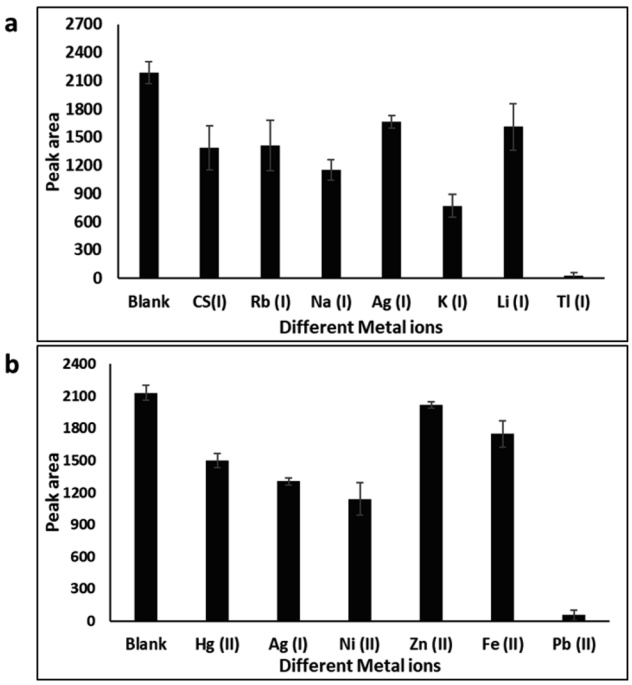

Fig. 8 (a) The AuNPs based LFA selectivity experiments for Tl(I) over K(I), Rb(I), Na(I), Cs(I), Ag(I) and Li(I). All the metal ions concentrations were 120 μM. (b) The AuNPs based LFA selectivity experiments for Pb(II) over Zn(II), Ag(I), Hg(II), Ni(II), and Fe(II). All the ion concentrations were 150 nM. Triplicate experiments were performed. The histogram of corresponding peak area (test (T) zone *vs.* various metal ions) were analyzed by ImageJ software.

As a practical application, the Tl(I) concentration in river water samples was measured using the LFA. The river water was filtered with a 0.22 μm filter membrane, boiled for 10 minutes, and then filtered again before use. Natural Tl(I) in the river water was too low to be detected by this LFA. The experiments were performed by spiking different concentrations (0–120 μM) of Tl(I) into river water (Fig. S11a†). A histogram was plotted from the test and control peak area *vs.* various Tl(I) concentrations (Fig. S11b†). This assay displayed a linearity with a LOD of 11.4 μM. Similarly, we developed an LFA for Pb(II) in river water using a AuNPs and Pb-binding aptamer. The histogram of corresponding test peak area *vs.* various concentrations of Pb(II) and the results showed the LOD of 5.3 nM (Fig. S11c and d†).

Likewise, the developed LFA was further used to detect Tl(I) in human serum samples (10%). The serum solution were prepared 1 : 10 (v/v) in water. Similar results were noticed to those for detection of Tl(I) spiked in serum sample (see Fig. S12a and b†). This LFA calibration curve was linear with a LOD of 10.46 μM. Similarly, we developed the LFA for Pb(II) in serum using a AuNPs and Pb(II)-binding aptamer. The calculated LOD using ImageJ peak area was 7.1 nM (Fig. S12c and d†). These results revealed that the LFA was suitable in practical applications for metal ion (Tl(I) and Pb(II)) detection.

Correspondingly, we performed the colorimetric LFA using AgNPs and Tl(I)-binding aptamer aptasensor for the detection Tl(I). The LFA results were similar to those of the AuNP based colorimetric LFA detection of Tl(I) experiments. The AgNP LFA test dot color intensity on the test region greatly decreased with

increasing concentrations (0 to 120 μM). A curve was plotted as the test (T) peak area *vs.* different concentrations of Tl(I) showing a linear range (0 M to 26 μM) Tl(I) with a calculated limit of detection of 6.3 μM (Fig. 9). Experiments were also performed using the LFA for Pb(II) and AgNPs and a Pb-binding aptamer sequence as depicted in Fig. S13a.† The results demonstrated a visual LOD of 33 nM (Fig. S13a†) and the AgNPs LFA ImageJ calculated LOD of 8 nM (Fig. S13b and c†). Overall, both metal nanoparticle LFA approaches were simpler than commonly performed colorimetric assays. LFA methods have various attractive detection properties, such as rapid experimental procedure within 30 minutes, cost efficiency, minimal training, and results that can be visually observed within 5 minutes.

The AgNPs based LFA selectivity experiments of Tl(I) were performed against a variety of metal ions: Ag(I), Cs(I), K(I), Na(I), Li(I) and Rb(I). Results showed the appearance of a yellow colored dot on the test area because of the accumulation of AgNP/aptamer complexes (Fig. S14a†). The observations indicate that the LFA is highly specific for Tl(I). Similarly, the LFA selectivity experiments for Pb(II) ions were performed with different metal ions such as Zn(II), Hg(II), Ag(I), Ni(II) and Fe(II) which led to the appearance of a yellow colored dot on the test zone due to the accumulation of aptamer–AgNP complexes (Fig. S14b†). The observations indicate that the LFA was highly specific for Pb. AgNP-based LFA detection of Tl and Pb in both river water and serum were also performed successfully (Fig. S15 and S16†). These results indicating that the LFA is useful in practical applications for metal ion (Tl(I) and Pb(II)) detection as well.

For comparison purposes, we reviewed many aptamer-based colorimetric, and lateral flow assay biosensors for toxic metal ions that used a variety of recognition materials (Table 1). These methods have shown LODs from 4.6 μM to 59 μM for Tl(I) and 702 pM to 500 nM for Pb(II).[7,47–49] Comparatively, Our LFA and colorimetric methods had low LODs (Table 1). In addition, both the Au and Ag nanoparticles-based LFAs reported herein have many benefits over colorimetric biosensors. The LFA method is relatively fast and with result interpretation that is easy for non-specialists. When both Au and Ag nanoparticle-based LFAs were compared, the drawbacks of the Ag nanoparticle LFA method was observed with a slight visual yellow color even without a target. This may be due to the formation of smaller agglomerates of metal nanoparticles on the LFA control and test spots. In addition, we performed the LFA experiments for toxic metal ions in 10% human serum, and river water. The LFAs permitted the detection of micromolar quantities of Tl(I) and nanomolar quantities of Pb(II) ions in the presence of other interfering

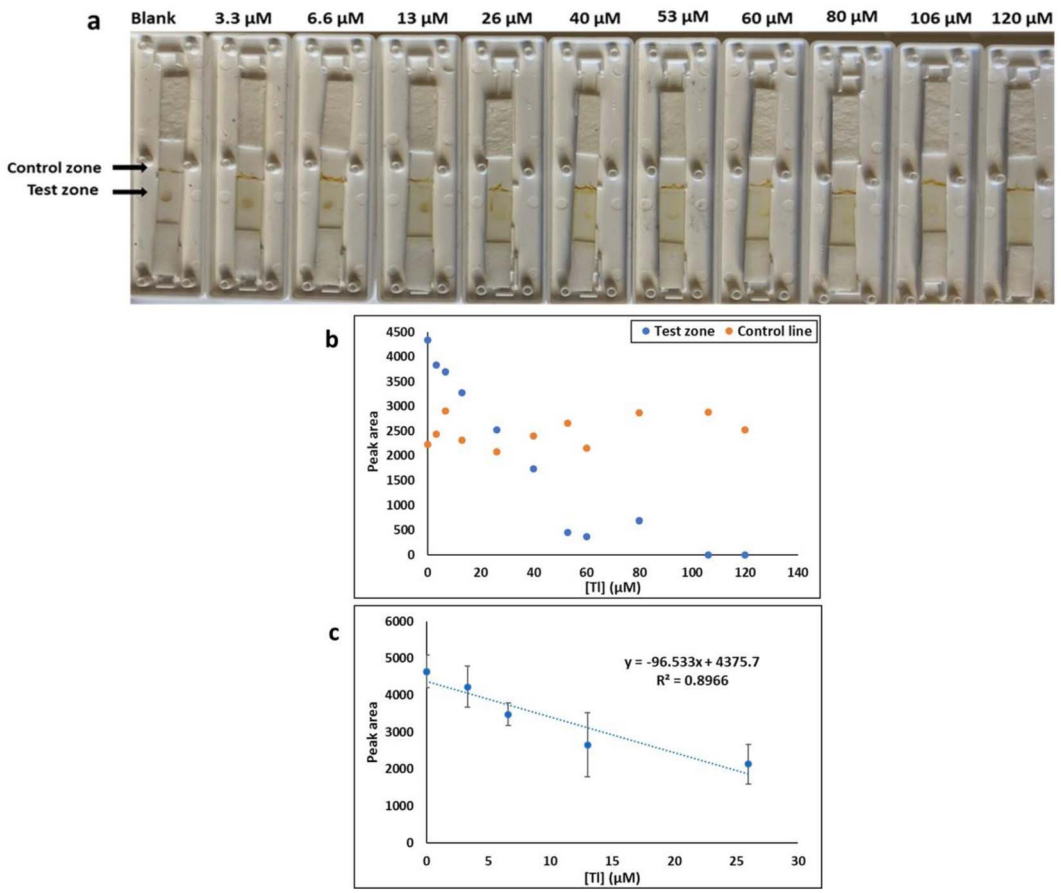

Fig. 9 (a) The LFA (AgNPs based) for Tl(I) (from 0–120 μM). (b) The curve was plotted against the peak area of test (T) and control (C) lines *vs.* various Tl(I) ions concentrations and were analyzed by ImageJ software. (c) Plot of the linear dynamic range.

Table 1 Comparison of various aptasensors (LODs) for Tl(I) and Pb(II)

Detection technique	Target	Method	LOD	Ref.
DNAzyme	Pb^{2+}	Microfluidic particle dam-eye	2.1 nM	50
DNAzyme	Pb^{2+}	Colorimetric	3 nM	51
DNAzyme	Pb^{2+}	Dipstick assay	0.05 nM	52
DNAzyme	Pb^{2+}	Dipstick assay	5 μM	49
Aptamer (complementary)	Pb^{2+}	Dipstick assay	2.5 nM	53
Aptamer (complementary)	Pb^{2+}	Dipstick assay	25 nM	48
Aptamer (label free)	Tl^{+}	Colorimetric	59 μM	7
Aptamer (label free)	Tl^{+}	Colorimetric (AuNP and AgNP)	9 μM, 3.2 μM	This work
Aptamer (label free)	Pb^{2+}	Colorimetric (AuNP and AgNP)	9.5 nM, 5.6 nM	
Aptamer (label free)	Tl^{+}	LFA (AuNP and AgNP)	7.4 μM, 6.3 μM	
Aptamer (label free)	Pb^{2+}	LFA (AuNP and AgNP)	6.6 nM, 8.0 nM	

metal ions, without any specialized instruments. The complete experiment only takes 30 minutes and therefore it can be suitable for practical applications for toxic metal ion detection in real samples.

4. Conclusions

In this study, we successfully established aptamer and nanomaterial-based assays for the detection of metal ions thallium(I) and lead(II). The first approach utilized adsorption–desorption aptasensor-based colorimetric detection of toxic metal ions using AuNPs and AgNPs. Lateral flow assays were the final method developed for rapid analysis of toxic metal ions with high affinity and selectivity. The LFAs produced results in minutes, which enabled an accurate and rapid detection of toxic metal ions. The result was assessed by visually noticing the changes of a red dot in the test zone. The LFA provided qualitative analysis by observed color changes and a semi-quantitative analysis *via* ImageJ software. Aptamer-based LFAs could be a rapid, inexpensive, and time efficient methodology providing high affinity and sensitivity, with the potential to become the basis for future biosensor devices. Future work should focus on toxic metal ions and small molecules in other LFA formats (*e.g.* fluorometric) to fully optimize the specificity, working range and binding capabilities of the aptamers.

Conflicts of interest

The authors declare no conflict of interest.

Acknowledgements

This work was financially supported by the Natural Sciences and Engineering Research Council of Canada (NSERC) grant RGPIN-2021-03817 awarded to Maria DeRosa.

References

1 H. Needleman, *Annu. Rev. Med.*, 2004, **55**, 209–222.
2 J. J. Rodríguez-Mercado and M. A. Altamirano-Lozano, *Drug Chem. Toxicol.*, 2013, **36**, 369–383.
3 A. L. J. Peter and T. Viraraghavan, *Environ. Int.*, 2005, **31**, 493–501.
4 V. K. Gupta and A. Rastogi, *J. Hazard. Mater.*, 2008, **152**, 407–414.
5 W. Zhang, B. Xiong, L. Chen, K. Lin, X. Cui, H. Bi, M. Guo and W. Wang, *Environ. Toxicol. Pharmacol.*, 2013, **36**, 51–57.
6 A. R. Shelke, J. A. Roscoe, G. R. Morrow, L. K. Colman, T. K. Banerjee and J. J. Kirshner, *Bone*, 2008, **23**, 1–7.
7 M. Hoang, P. J. J. Huang and J. Liu, *ACS Sens.*, 2016, **1**, 137–143.
8 O. T. Butler, J. M. Cook, C. F. Harrington, S. J. Hill, J. Rieuwerts and D. L. Miles, *J. Anal. At. Spectrom.*, 2006, **21**, 217–243.
9 S. Galván-Arzate and A. Santamaría, *Toxicol. Lett.*, 1998, **99**, 1–13.
10 H. Kuang, C. Xing, C. Hao, L. Liu, L. Wang and C. Xu, *Sensors*, 2013, **13**, 4214–4224.
11 N. L. Rosi and C. A. Mirkin, *Chem. Rev.*, 2005, **105**, 1547–1562.
12 M. E. Stewart, C. R. Anderton, L. B. Thompson, J. Maria, S. K. Gray, J. A. Rogers and R. G. Nuzzo, *Chem. Rev.*, 2008, **108**, 494–521.
13 Y. Song, W. Wei and X. Qu, *Adv. Mater.*, 2011, **23**, 4215–4236.
14 J. S. Lee, A. K. R. Lytton-Jean, S. J. Hurst and C. A. Mirkin, *Nano Lett.*, 2007, **7**, 2112–2115.
15 A. Ellington and J. W. Szostak, *Nature*, 1990, **346**, 818–822.
16 C. Tuerk and L. Gold, *Science*, 1990, **249**, 505–510.
17 J. Qu, S. Yu, Y. Zheng, Y. Zheng, H. Yang and J. Zhang, *Cell. Mol. Life Sci.*, 2017, **74**, 683–695.
18 D. Shangguan, L. Meng, Z. C. Cao, Z. Xiao, X. Fang, Y. Li, D. Cardona, R. P. Witek, C. Liu and W. Tan, *Anal. Chem.*, 2008, **80**, 721–728.
19 J. G. Bruno, M. P. Carrillo, A. M. Richarte, T. Phillips, C. Andrews and J. S. Lee, *BMC Res. Notes*, 2012, **5**, 633.
20 J. A. Latham, R. Johnson, J. J. Toole, G. Sciences, L. Drive and F. City, *Oligonucleotides*, 1994, **22**, 2817–2822.
21 C. Wilson, J. Nix and J. Szostak, *Biochemistry*, 1998, **37**, 14410–14419.
22 C. Reinemann, U. Freiin von Fritsch, S. Rudolph and B. Strehlitz, *Biosens. Bioelectron.*, 2016, **77**, 1039–1047.
23 K. Feng, Y. Kang, J. J. Zhao, Y. L. Liu, J. H. Jiang, G. L. Shen and R. Q. Yu, *Anal. Biochem.*, 2008, **378**, 38–42.

24 S. Centi, S. Tombelli, M. Minunni and M. Mascini, *Anal. Chem.*, 2007, **79**, 1466–1473.
25 Y. Wang, Y. Wang and B. Liu, *Nanotechnology*, 2008, **19**, 415605–415611.
26 Z. Chen, G. Li, L. Zhang, J. Jiang, Z. Li, Z. Peng and L. Deng, *Anal. Bioanal. Chem.*, 2008, **392**, 1185–1188.
27 Y. Huo, L. Qi, X. J. Lv, T. Lai, J. Zhang and Z. Q. Zhang, *Biosens. Bioelectron.*, 2016, **78**, 315–320.
28 J. Wang, J. Lu, S. Su, J. Gao, Q. Huang, L. Wang, W. Huang and X. Zuo, *Biosens. Bioelectron.*, 2015, **65**, 171–175.
29 D. Li, S. Wei, H. Yang, Y. Li and A. Deng, *Biosens. Bioelectron.*, 2009, **24**, 2277–2280.
30 Y. Y. Lin, J. Wang, G. Liu, H. Wu, C. M. Wai and Y. Lin, *Biosens. Bioelectron.*, 2008, **23**, 1659–1665.
31 S. Wang, Y. Quan, N. Lee and I. R. Kennedy, *J. Agric. Food Chem.*, 2006, **54**, 2491–2495.
32 Y. J. Cho, D. H. Lee, D. O. Kim, W. K. Min, K. T. Bong, G. G. Lee and J. H. Seo, *J. Agric. Food Chem.*, 2005, **53**, 8447–8451.
33 R. Velu and M. C. De Rosa, *Analyst*, 2018, **143**, 4566–4574.
34 J. Liu, J. Zeng, Y. Tian and N. Zhou, *Analyst*, 2018, **143**, 182–189.
35 J. Zhang, Z. Shen, Y. Xiang and Y. Lu, *ACS Sens.*, 2016, **1**, 1091–1096.
36 Z. Wu, H. Shen, J. Hu, Q. Fu, C. Yao, S. Yu, W. Xiao and Y. Tang, *Anal. Bioanal. Chem.*, 2017, **409**, 5209–5216.
37 S. M. Taghdisi, N. M. Danesh, P. Lavaee, A. S. Emrani, M. Ramezani and K. Abnous, *RSC Adv.*, 2015, **5**, 43508–43514.
38 S. M. Taghdisi, S. S. Emrani, K. Tabrizian, M. Ramezani, K. Abnous and A. S. Emrani, *Environ. Toxicol. Pharmacol.*, 2014, **37**, 1236–1242.
39 C. A. Schneider, W. S. Rasband and K. W. Eliceiri, *Nat. Methods*, 2012, **9**, 671–675.
40 P. Alivisatos, P. F. Barbara, A. W. Castleman, J. Chang, D. A. Dixon, M. L. Klein, G. L. McLendon, J. S. Miller, M. A. Ratner, P. J. Rossky, S. I. Stupp and M. E. Thompson, *Adv. Mater.*, 1998, **10**, 1297–1336.
41 T. Kippeny, L. A. Swafford and S. J. Rosenthal, *J. Chem. Educ.*, 2009, **79**, 1094.
42 D. H. J. Bunka and P. G. Stockley, *Nat. Rev. Microbiol.*, 2006, **4**, 588–596.
43 O. Doluca, J. M. Withers and V. V. Filichev, *Chem. Rev.*, 2013, **113**, 3044–3083.
44 C. Zong and J. Liu, *Anal. Chem.*, 2019, **91**, 10887–10893.
45 V. Ranganathan, S. Srinivasan, A. Singh and M. C. DeRosa, *Anal. Biochem.*, 2020, **588**, 113471.
46 O. A. Alsager, S. Kumar and J. M. Hodgkiss, *Anal. Chem.*, 2017, **89**, 7416–7424.
47 S. M. Taghdisi, N. M. Danesh, P. Lavaee, M. Ramezani and K. Abnous, *Environ. Toxicol. Pharmacol.*, 2015, **39**, 1206–1211.
48 D. Wang, C. Ge, K. Lv, Q. Zou, Q. Liu, L. Liu, Q. Yang and S. Bao, *Chem. Commun.*, 2018, **54**, 13718–13721.
49 D. Mazumdar, J. Liu, G. Lu, J. Zhou and Y. Lu, *Chem. Commun.*, 2010, **46**, 1416–1418.
50 G. Wang, L. T. Chu, H. Hartanto, W. B. Utomo, R. A. Pravasta and T. H. Chen, *ACS Sens.*, 2020, **5**, 19–23.
51 Z. Wang, J. H. Lee and Y. Lu, *Adv. Mater.*, 2008, **20**, 3263–3267.
52 X. Pei, *Chem. Lett.*, 2014, **43**, 1643–1644.
53 H. B. Wang, L. H. Ma, B. Y. Fang, F. Tan, Y. C. Cao, Y. Di Zhao and X. Bin Hu, *Sens. Actuators, B*, 2018, **261**, 307–315.